Metastable zinc-blende MgS structure: Combined experimental and theoretical study

C. Bocchi,* A. Catellani, F. Germini, and L. Nasi
CNR-IMEM Institute, Parco Area delle Scienze 37/A, I-43100 Parma, Italy

J. K. Morrod† and K. A. Prior
School of Engineering and Physical Sciences, Brewster Building, Heriot-Watt University, Edinburgh EH14 4AS, United Kingdom

G. Calestani
Department of Chemistry, Parma University, Parco Area delle Scienze 17/A, I-43100 Parma, Italy
(Received 9 January 2009; revised manuscript received 28 April 2009; published 5 June 2009)

MgS/ZnSe/GaAs multilayers with the MgS thickness ranging from 20 to 140 nm were grown at 300 °C by molecular-beam epitaxy on [001] GaAs substrates. The samples were studied by using several x-ray methods and transmission electron microscopy. The coexistence of metastable zinc-blende (ZB) and rocksalt MgS structural phases was evidenced and discussed. The analysis of reciprocal space maps of the x-ray intensity distribution around asymmetrical reciprocal-lattice nodes allowed us to determine the strain status of the MgS layers and to show that the ZB-MgS phase was pseudomorphic also in the case of the thickest film. The lattice parameter of the pure ZB-MgS phase ranging between $0.563\ 33 < a_{\mathrm{MgS}} < 0.563\ 67$ nm was obtained by extrapolation from x-ray diffraction data and predicted *ab initio* elastic constants, taking into account that there was a Zn incorporation during the MgS growth estimated in the range $0.005 \leq x_{\mathrm{Zn}} \leq 0.02$.

DOI: 10.1103/PhysRevB.79.235310 PACS number(s): 61.05.cp, 62.20.dq, 31.15.es, 64.70.kg

I. INTRODUCTION

In recent years it has been demonstrated that it is possible to grow epitaxial compounds in a crystallographic phase different from their lowest-energy configuration using thin-film growth techniques such as molecular-beam epitaxy (MBE) (Refs. 1 and 2) and metal-organic chemical vapor deposition (MOCVD).[3,4] This is particularly true for II-VI semiconductor materials including the important wide band-gap semiconductor MgS. Although the stable structure of MgS is rocksalt (RS), the crystal symmetry of the underlying material induces a metastable zinc-blende (ZB)-MgS configuration (β-MgS) in the layer while changing the coordination environment from sixfold to fourfold. ZB MgS has been successfully used as a wide gap barrier material giving effective confinement in the II-VI quantum well[3,5,6] and quantum dots structures.[7,8] The interest in this material for optoelectronic applications is mainly associated with its metastable ZB phase in epitaxial structures. Hence, the control of the growth method, the knowledge of the material mechanical properties when in the ZB configuration, and specifically, of the elastic constants and the lattice parameter, as well as strain release and structural phase change mechanisms, are prerequisites for the promising use of β-MgS in electronic device developments.

The renewed attention to this compound has promoted several theoretical and experimental works over the last years with the aim to investigate the electronic properties and to determine the most important structural parameters of the metastable phase. First-principles studies gave a significant broad spectrum of β-MgS elastic moduli and lattice cell constant values (a review will be given in Table III). On the other hand, direct measurements of these parameters are reported in a few works and the experimental results do not always match satisfactorily with the calculated values. Since bulk MgS crystallizes with the rocksalt structure and it does not exist as a ZB free-standing material, this represents a further complication for experimental investigations which have to do only with MgS layers embedded in epitaxial structures. Therefore, the knowledge of the strain status of the material and its relationship with the structural phase transition from the metastable ZB to RS is crucial for an accurate determination of the lattice parameters.

The measurement and calculation of these parameters in the ZB-MgS/ZnSe/GaAs system are the aim of this study. Suitable heterostructures were prepared by MBE and analyzed by using different techniques based on x-ray diffraction (XRD), x-ray topography, and x-ray reflectivity, including the mapping of the x-ray intensity distribution in the reciprocal space map (RSM) for the strain determination. Furthermore, both XRD and transmission electron microscopy (TEM) investigations are carried out to detect the occurrence of the phase change and its relation with the presence of extended defects in the material. The experimental findings are compared with the results of *ab initio* calculation performed within the density-functional theory (DFT). In the end, we discuss our results in comparison with previously published data.

II. EXPERIMENTAL AND COMPUTATIONAL DETAILS

The samples used in this study were grown by MBE using a method which we have described previously[2,6] in which MgS is deposited using sources of elemental Mg and sulfur supplied from a compound ZnS source. In order to produce material of acceptable quality using this technique, all structures grown on GaAs substrates commence with a thin ZnSe-buffer layer. Following the removal of the oxide layer from the GaAs substrate surface prior to growth, it is necessary to reduce, as much as possible, the reaction of the GaAs surface with the background sulfur in the system. In our system, this

is accomplished by using a liquid nitrogen cooled shutter in front of the ZnS source, and additionally irradiating the GaAs surface while it is cooling down to the growth temperature with a zinc flux.[9,10] During the clean up of the sample surface and subsequent growth of the structures, the sample surface is routinely monitored by reflection high-energy electron diffraction, with the growth of ZnSe occurring under near-stoichiometric conditions while the growth of MgS takes place under highly metal-rich conditions. The growth rates of the ZnSe and MgS layers were very low, as is usual in the deposition of MgS. From the deposition times they were determined to be 0.05 and 0.06 nm s^{-1}, respectively.

Two [001]-oriented GaAs/ZnSe(30 nm)/MgS(18 nm)/ZnSe(15 nm)/MgS(t nm)/ZnSe(7.5 nm) multilayer samples with upper MgS layer thicknesses $t=140$ nm (sample 1) and $t=40$ nm (sample 2), and two GaAs/ZnSe(30 nm)/MgS(t nm)/ZnSe(7.5 nm) simpler structures with MgS layer thicknesses $t=40$ nm (sample 3) and $t=20$ nm (sample 4), were grown at 300 °C. This temperature is higher than our previous growth temperature range (240–270 °C) for MgS and is close to the maximum temperature at which this material can be successfully deposited. The samples were capped with a 7.5-nm-thick layer of ZnSe in order to prevent the degradation of the hygroscopic MgS layers. At the bottom of samples 1 and 2, the ZnSe(30 nm)/MgS(18 nm)/ZnSe(15 nm) multilayer replaces the single ZnSe (30 nm) buffer layer used for samples 3 and 4 with the aim of increasing the crystal quality of the whole structure.[11]

The samples were investigated by using a Philips X'Pert high-resolution x-ray diffractometer (HRXRD) equipped with a graded multilayers mirror to increase the intensity of the incidence x-ray beam and with two channel-cut Ge crystals set for the Cu $K\alpha_1$ 220 reflections as a monochromator. The diffraction profiles of the symmetric 004 ($R=0,\pi$) Bragg reflection with the azimuthal angle R differing by π were collected in the ω-2θ scan mode from each sample. By this procedure it was possible to eliminate the effect of any miscut angle. The analysis of the diffraction profiles for the fully strained samples was carried out by means of an algorithm based on the theoretical approach developed by Takagi[12] and Taupin[13] for elastically deformed crystals which constitutes a generalization of the dynamical x-ray diffraction theory.[14] In order to increase the quality of the fits it was necessary to account for the diffused scattering due to both thermal vibrations and crystal lattice imperfections. The thermal diffuse scattering is completely incoherent and it was possible to approximate it by a suitable piecewise-smooth function. The fitting procedure was based on the minimization of the parameter χ^2 given by the squared difference between experimental and calculated values of the diffracted intensity, normalized by the degrees of freedom $r=n-p$ of the system, where n is the number of experimental points and p is the number of layer parameters describing the structures. Thus, the thickness of each layer, a Debye-Waller factor accounting for the static disorder, and the perpendicular component of lattice mismatch $\Delta d/d^{\perp}=(d_L-d_S)/d_S$ (where d_L and d_S are the spacing in the layer and substrate lattices, respectively) could be obtained. The coherent intensity distribution in reciprocal space, that is, RSM, was measured around asymmetrical nodes. The intensity maps were collected using the same diffractometer with a three bounce channel-cut Ge analyzer crystal in front of the detector for separating the coherent component of the scattered radiation from the incoherent one. The strain status of the samples was determined by the analysis of the reciprocal space maps. The powder diffractometry technique was also used to detect the presence of the MgS RS phase by making ω-2θ scans along the [001] reciprocal-lattice direction in a large angular range, suitable for including the 002 and 004 reflections. Double crystal x-ray topography was performed on all samples as a nondestructive screening technique to check the presence of misfit dislocations or other extended defects. Sample 1 with the thicker MgS upper layer was also analyzed by the x-ray reflectivity technique, taking advantage from the property that in the reflectivity regime, due to the very small incident angles of the typical measurement range, the scattering vector remains very close to the origin of the reciprocal space and the strain sensitivity vanishes. TEM analysis both in plain view and cross-section geometries was carried out using a Jeol 2000FX microscope working at 200 kV.

The calculations[15] were performed in the frame of DFT, adopting the local-density approximation (LDA). Electron-ion interactions were included through fully nonlocal ultrasoft pseudopotentials.[16] The single-particle wave functions (charge density) are expanded in a plane-wave basis set up to a cutoff energy of 30 Ry (300 Ry). We verified that using generalized gradient approximation (GGA) corrections (in the PW91 approximation[17]) does not sensibly affect the results presented in terms of relative differences of lattice parameters. In this frame, we performed a set of simulations of the lattice parameter of the different zinc-blende and rocksalt structures, with a converged $12\times12\times12$ Monkhorst-Pack grid[18] $\boldsymbol{k}$-point sampling of the Brillouin zones, thus allowing energy comparison of the different cubic and pseudomorphic structures. Test calculations were performed at 50 Ry cutoff for the description of the electronic wave function (500 Ry for charge density) and $12\times12\times12$ $\boldsymbol{k}$-point grid. Beyond assessing the accuracy of our results, these tests were required to obtain the elastic constants of the ideal crystal structures at equilibrium, in the LDA approximation, since it is known that stress contributions are slowly convergent terms. ZnMgS alloys were also considered, and calculations (50 Ry cutoff, $12\times12\times12$ $\boldsymbol{k}$-point grid) for 1/32 and 2/32 ZnMgS alloys were performed in the virtual-crystal approximation, where Zn is supposed to be a substitute of Mg atoms.

III. RESULTS AND DISCUSSION

A. Structural phase change

The metastable ZB MgS is nearly lattice matched to both GaAs and ZnSe, with the lattice parameter $a_{\beta\text{-MgS}}<a_{\text{GaAs}}<a_{\text{ZnSe}}$, allowing the formation of strain balanced structures. Indeed, it has been shown[6] that MgS layers up to 140 nm thick of good crystal quality can be grown by MBE in the ZB structure lattice matched to GaAs on top of a ZnSe buffer. In the case of an heteroepitaxial system the recovering of the stable RS-MgS phase can occur when certain criti-

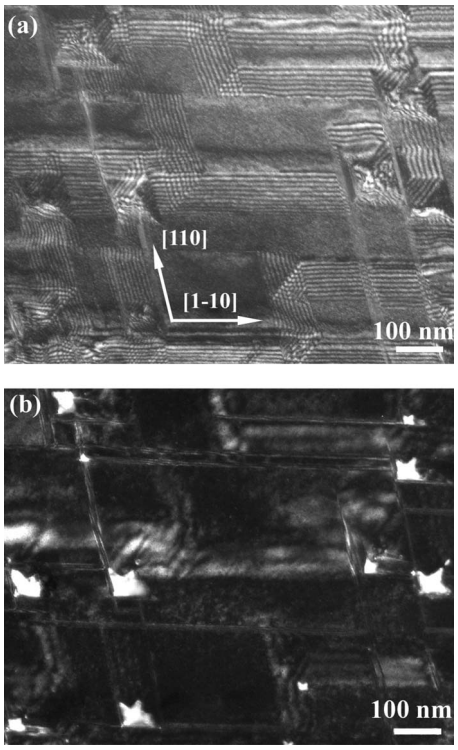

FIG. 1. TEM plan view micrographs of sample 1 taken close to the 45°-inclined [110] zone axis with (a) $\mathbf{g}=1-11$ and (b) $\mathbf{g}=200$. The bright regions in Fig. 1(b) correspond to the RS grains at the crossing stacking faults.

cal conditions are satisfied: strain,[11] growth temperature,[19,20] presence of defects, etc. Although the onset of the structural transition seems to be related to the existence of a critical thickness,[21] the mechanisms governing the ZB to RS transformation in heterostructures are also complex depending on the crystal quality as well as on the unintentional doping (by diffusion or direct incorporation) of the grown materials.

In a preliminary work, we have recently discussed the manifestation of the MgS structural transition from metastable zinc-blende to rocksalt crystal in the MgS/ZnSe/GaAs multilayer system.[22] In particular, samples 1 and 2 investigated in the present work were also analyzed in that context and the coexistence of both rocksalt and zinc-blende MgS structural phases was experimentally detected. In summary, a partial nucleation of MgS rocksalt was evidenced by both x-ray diffraction measurements and TEM investigations and the phase change was correlated with the presence of a high density of stacking faults as evidenced by TEM images. Indeed, it was shown that when the stacking faults lying on different glide planes intersect, they produce favorable sites for the transition from the metastable ZB phase to the stable RS bulk structure. The RS phase grows only in the limited region confined by the crossing stacking faults and the RS crystallites, thus expand in a star-pyramidal shape having each of the four arms along the directions where the planar defects intersect, i.e., the ⟨011⟩-type directions inclined to the growth surface. Figure 1 shows the plan view TEM images of sample 1 taken close to the 45°-inclined [110] zone axis, under different diffraction conditions. The remarkable correspondence between the RS clusters and the crossing stacking faults is clearly exhibited in the two micrographs obtained by using the operative reflections $\mathbf{g}=1-11$ [Fig. 1(a)] and $\mathbf{g}=200$ [Fig. 1(b)] to enhance the ZB and RS phases, respectively. The contribution from the rocksalt structure comes from the star-shaped grains which appear significantly brighter than the surrounding regions [Fig. 1(b)] due to the high value of the RS structure factor of the (200) reflection compared to the ZB phase.

The coexistence of both rocksalt and zinc-blende MgS structural phases was confirmed in samples 1 and 2 by x-ray diffraction experiments and by using a powder-diffraction setup in order to collect the whole scattered intensity also in the case of an appreciable deterioration of the crystal quality (see Ref. 22). The results obtained for samples 1 and 2 supported the presence of RS-MgS phase. To improve and complete the structural analysis of this system, x-ray RSMs and ω-2θ scans with HRXRD setup, has been performed. It should be noted that a [001]-oriented crystal with the RS structure gives the strongest x-ray diffraction intensity for the 002 Bragg reflection, while for the same crystal orientation, but with the ZB structure, the 004 is the strongest Bragg reflection.[23] The result obtained for sample 1 is shown in Fig. 2: (a) the logarithm in base 10 of diffracted intensity collected by ω-2θ scan through the 002 reflection of each layer of the structure and (b) the RSM collected around the 002 node of the substrate reciprocal lattice. The [001] direction is marked in Fig. 2(b) by a dashed line. Actually, HRXRD ω-2θ scan does not add information but makes easier the identification of each contribution and the peak intensity broadening along the scan direction. The intensity distribution perpendicular to the [001] direction is related to the mosaic spread of the crystal lattice.[24] The width of the RS-MgS 002 peak shows a spread of about 1° as confirmed also by TEM-selected area diffraction pattern (not shown here). The intensity is very low but this is due to its distribution over a large area (mosaic effect). In conclusion, the coexistence of both rocksalt and zinc-blende MgS structural phases could be justified taking into account that the free energy for the RS to ZB phase transition of MgS is very low because the large Philips' ionicity places it very close to the boundary between the regions of stability for the two phases.[25] A schematic of this structural transition is sketched in Fig. 3.

In samples 3 and 4 the RS phase was not detected. This is not surprising for sample 4 which has the thinnest MgS layer ($t=20$ nm) of the sample series, with this thickness being also very close to the limit of sensitivity of the XRD conventional techniques. Furthermore, the occurrence of the phase transition should initially affect only a part of the layer as evidenced in the first two samples and strictly depends on the density of stacking faults and on their interaction.

In sample 3 the MgS layer is 40 nm thick, similar to sample 2 where the RS phase was found. However, the two samples differ in that sample 2 has a buffer layer. As pointed out in Ref. 6 the ZnSe(30 nm)/MgS(18 nm)/ZnSe(15 nm) multilayer grown as a buffer in samples 1 and 2 increases the crystal quality of the whole structure with respect to the use of a single ZnSe-buffer layer.[6] This result could be confirmed by the comparison between samples 2 and 3. Any degradation of the crystal quality produces a broadening of the diffraction angular range and a consequent lowering of the peak

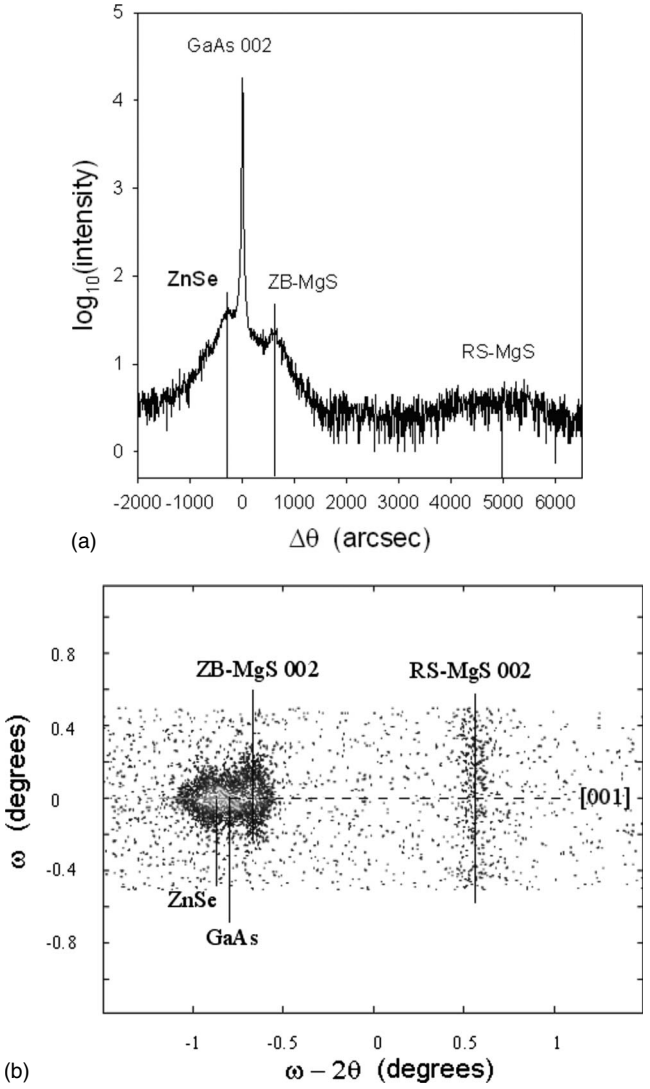

FIG. 2. (a) Sample 1: logarithm in base 10 of the 002 Cu $K\alpha_1$ diffracted intensity vs the deviation from the substrate Bragg-peak angular position ($\Delta\theta$) collected in ω-2θ scan mode along the [001] direction. (b) RSM collected around the 002 reciprocal-lattice node; the dashed line marked in the figure is coincident with the [001] direction. The markers (solid lines) perpendicular to the [001] direction give the ZnSe, GaAs, ZB-MgS, and RS-MgS 002 nodes position, respectively. The intensity broadening along the marker direction is due to the mosaic misorientation.

intensity until it becomes no longer detectable. This consideration will be supported by the analysis of further HRXRD measurements given in the next paragraphs.

B. Strain

It is a common knowledge that the reciprocal lattice of a heteroepitaxial system is a superposition of the layer and the substrate reciprocal lattice respectively. When a layer is elastically deformed at the first epitaxial growth stage (pseudomorphic growth), its reciprocal lattice lines up to the substrate nodes along the surface-normal direction. Beyond a given critical thickness the strain relaxation starts and the

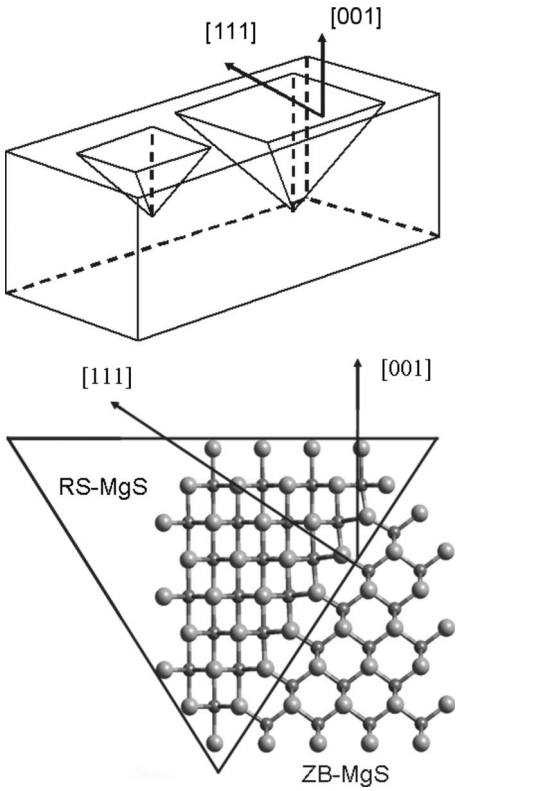

FIG. 3. Schematic of the change in phase occurring at the intersection between stacking faults lying on different (111) glide planes. (a) RS-MgS cores grow initially limited by a pyramid-shaped sites; (b) RS phase maintains the [001] orientation of the original ZB lattice.

layer nodes move to the positions corresponding to its unstrained (fully relaxed) lattice. At the end of the relaxation process the crystallographic directions of the two lattices must be aligned. Under the general assumption that Hook's law is obeyed during the relaxation, the path covered by the lattice nodes between the initial and final points of the process is a straight line. The strain status of the layer is then determined by the position of its reciprocal-lattice node along this straight path. In a conventional single or double crystal diffraction experiment all the radiation scattered by the sample is integrated along the acceptance angle of the detector. This is responsible for an overlap of the different contributions to the intensity diffraction profile. Mosaic misorientation, disorder, bending, composition gradients, and strain broaden the intensity distribution in the reciprocal space along different directions. According to Fewster[24,26] and Heinke *et al.*,[27] a RSM of the scattered intensity, obtained by combining ω- and ω-2θ scan modes, enables the separation of these contributions.

The coherent intensity distribution in the reciprocal space was measured around the 224 asymmetrical nodes in both the glancing incidence (ω^-, -224) and glancing emergence (ω^+, $2-24$) geometries. The RSM of the asymmetrical -224 reflection of sample 1 is shown in Fig. 4 in reciprocal space coordinates (q_z, q_x) to allow an immediate identification of the major crystallographic directions and the correct representation of the intensity contours. The conversion from the

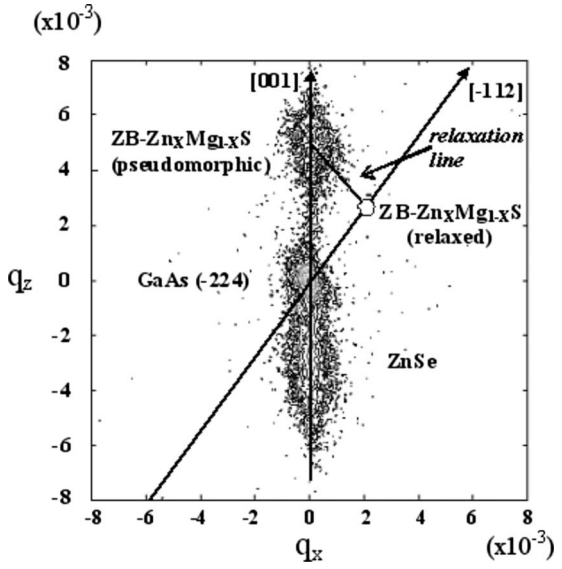

FIG. 4. Asymmetrical −224 Cu $K\alpha_1$ RSM of sample 1 shown in reciprocal space coordinates. The intensity distribution is positioned along a direction perpendicular to the surface (parallel to [001]). This means that the (ZB) $Zn_XMg_{1-X}S$ layer $(0.02 \leq x \leq 0.03)$ is pseudomorphic. The position of the −224 node on the [112] direction in the case of unstrained (relaxed) lattice is also shown.

angular $(\omega,\ 2\theta)$ to reciprocal space coordinates is given by $q_x = R[\cos(\omega) - \cos(2\theta - \omega)]$ and $q_z = R[\sin(\omega) - \sin(2\theta - \omega)]$, where R is the Ewald sphere radius $R = |\boldsymbol{k}_{i,s}| = 2\pi/\lambda$, $\boldsymbol{k}_i$ and $\boldsymbol{k}_s$ are the incident and scattered wave vectors, respectively, and λ is the x-ray wavelength.

Sample 1 presents the thickest MgS layer, and a fair chunk of the layer exhibits the zinc-blende structure as demonstrated in the previous paragraph. The scattered intensity of the whole structure is distributed along a direction perpendicular to the surface (i.e., parallel to the [001] substrate direction). This leads to the conclusion that both ZnSe and ZB-MgS layers are strained or at a very early stage of relaxation. This last hypothesis must be taken into account because of the presence of a high density of stacking faults as evidenced by TEM investigations, even if the dislocations bordering the stacking faults are poorly effective to release the strain. On the other hand, no misfit dislocations have been detected by x-ray topography measurements in any of the samples, confirming that the MgS lattice relaxation does not take place at least through the usual mechanism for which the release of the strain energy is accompanied by the generation of these extended defects. The broadening of the ZnSe intensity along q_z is due to the overlap of the contributions coming from the ZnSe buffer and the ZnSe-top layer. As a matter of fact, the latter is subject to a different growth condition with respect to the buffer because it grows on the MgS surface where some islands of MgS rocksalt phase crop out, as pointed out above. Therefore, as a first conclusion we have evidenced that the two MgS phases can coexist and also that the lattice of ZB phase is pseudomorphic. The strain status of the RS-MgS phase was not determined due to the low and broadened intensity of the 002 RS peak as shown in both RSM and ω-2θ scan of Fig. 2.

C. ZB-MgS lattice parameter

The analysis and discussion of experimental results drawn up to here allow us to determine the lattice parameter of the ZB-MgS phase. Figure 5 shows the 004 diffracted intensity profiles, in logarithmic in base 10 scale vs the deviation from the substrate Bragg-peak angular position, of all samples and the relating fittings obtained with the trends of the mismatch perpendicular component vs depth shown in the figures. Sample 1 [Fig. 5(a)] fits better for the purpose of this section, and it will be analyzed after a preliminary discussion of the results obtained for the other samples.

Both samples 2 and 3 have a 40 nm MgS thick top layer and they differ in the buffer layer as already mentioned. The balancing of the strain in the former case should improve the crystal quality and this is the aim to use a ZnSe/MgS/ZnSe multilayer as a buffer. However, the comparison between sample 2 [Fig. 5(b)] and sample 3 [Fig. 5(c)] does not provide crucial evidence of an effective structural improvement. In similar samples previously grown in the optimum temperature range[6] (230–270 °C), the increase in the MgS thickness which could be deposited before the conversion from ZB to rocksalt occurred was observed to increase substantially from 67 to 140 nm. One possibility for the increase in critical thickness with a ZnSe/MgS/ZnSe multilayer buffer might be that the strain compensation was quite effective. This hypothesis seems to be confirmed in the present case by the reciprocal space map collected from sample 1 with the thickest MgS layer. Indeed the result (see Fig. 4) shows that the thicker portion of the layer exhibits the zinc-blende structure in pseudomorphic strain state. However, simultaneously, the relatively higher growth temperature used in this context can be considered responsible for a partial degradation of the MgS crystal quality, as this is the only parameter which has changed with respect to the previous growths. This degradation is connected with the high density of stacking faults detected, the coexistence of the two phases in the same layer and a possible change in the surface roughness. The last hypothesis might be confirmed observing that both mismatch profiles of samples 2 [Fig. 5(b)] and 3 [Fig. 5(c)] show some broadening at the interfaces and different strain values for the ZnSe-top layer with respect to that of the buffer. This result is common also to the other samples. In the presence of the step model adopted by the fitting program, we can read the behavior as a consequence of a worsening of the growth surface consistent with the mosaic spread showed by the RSMs. Furthermore, the fitting of the diffraction profiles gave a lower static Debye-Waller factor (DW, not shown here) associated with the MgS layers and ZnSe-top layers, suggesting that some loss of crystal quality occurs during the growth. Sample 2 shows a partial change in the structural phase of the MgS top layer as discussed before in Sec. III A, which can accentuate the lattice disorder evidenced by the DW. No evidence of the same switchover was detected in sample 3. As pointed out above, the x-ray topography did not detect misfit dislocations also in the case of these samples, confirming the conclusion that we cannot suppose the occurrence of strain release, but just a limited mosaic spreading also induced by the presence of a high density of stacking faults originated from the ZnSe-buffer layer[28,29] and common to all samples.

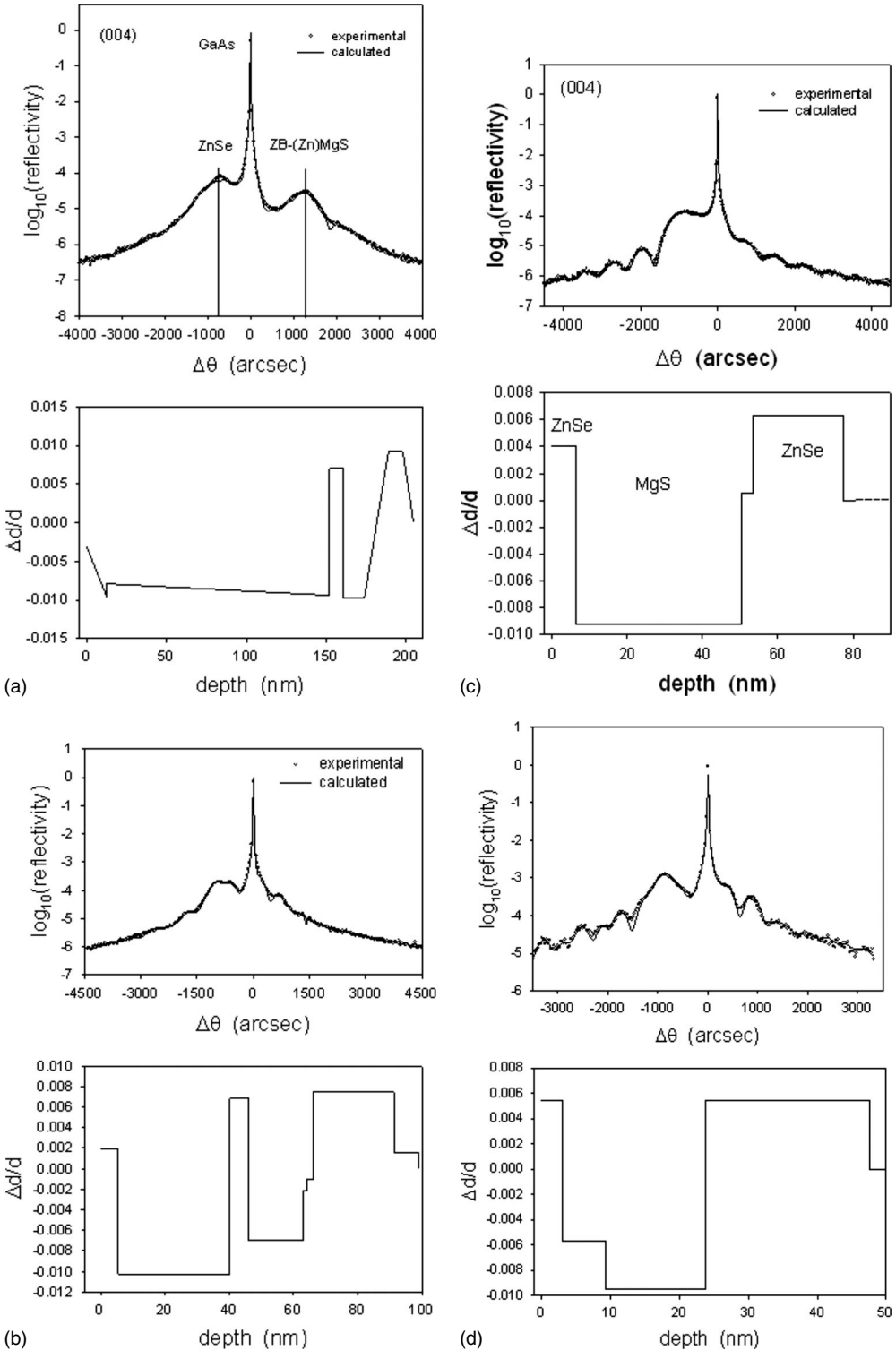

FIG. 5. Logarithm in base 10 of 004 Cu $K\alpha_1$ diffracted intensity (spot) of all the samples and relating fittings (solid line) obtained with the trends of the mismatch perpendicular component ($\Delta d/d$) vs *depth* shown in the figures. The figures are relative: (a) sample1; (b) sample 2; (c) sample3; (d) sample 4.

Sample 4 contains a 20 nm MgS thick layer. Although this MgS layer is very thin, the fitting of the diffraction profile [Fig. 5(d)] accompanied with a low DW suggests that the crystal quality is not completely satisfactory. Excluding strain release effects, some deviations from the ideal crystal quality of the MgS layer might be attributed to the relatively high growth temperature used in this context for the reasons discussed above regarding structures 2 and 3.

A possible incorporation of Zn into the MgS layer must take into account, since ZnS was used as a source of sulfur for growing MgS. Although in the MBE system the residual sulfur pressure is kept out, helped by a nitrogen cooled shut-

TABLE I. Experimental results obtained by x-ray diffraction data and by using our *ab initio* $\nu_{\text{ZB-MgS}}=0.433$ and $\nu_{\text{ZB-ZnS}}=0.334$ calculated values.

(*hkl*)	$\langle(\Delta a/a)^{\perp}\rangle$	x_{Zn}	$a_{\text{ZB-(Zn)MgS}}$ (nm)	a_{MgS} (nm)
004	-9.485×10^{-3}, $\pm5\times10^{-5}$	0.005	$x=0.005$, $\nu=0.432$, 0.56322	0.56333 ± 0.000015
−224		0.02	$x=0.02$, $\nu=0.431$, 0.563217	0.56367 ± 0.000015

ter in front of the ZnS source, a small part of the impinging Zn flux is inevitably incorporated into the growing layer. Secondary ion mass spectrometry (SIMS) and Auger measurements were carried out in samples grown at slightly lower temperatures. A slight Zn doping of the samples was found and quoted in the range 0.5%–2%.[2] The residual Zn level would be expected, on thermodynamic grounds, to decrease with increasing growth temperature, and this is confirmed by the growth by the Heriot-Watt MBE group of high Zn mole fraction ZnMgS alloys which require far lower growth temperatures.[30] The SIMS and Auger values can, therefore, be considered as upper bounds on the Zn mole fraction in the material examined in the present study and these values will be a reference data in the course of the following x-ray experimental analysis.

Sample 1 is the more suitable for determining the ZB-MgS lattice parameter because (i) the MgS layer is adequately thick as confirmed by the diffraction profile [Fig. 5(a)] fitting; (ii) the bulk of the MgS layer exhibits the zinc-blende structure and shows an acceptable crystal quality; (iii) the strain status of the zinc-blende lattice is pseudomorphic as found by the 224-RSMs (see Fig. 4). Although we are dealing with a $Zn_XMg_{1-X}S$ alloy instead of binary MgS, as underlined above, it is still possible to determine the lattice parameter of the pure ZB-MgS phase by extrapolation from the alloy mismatch components measured in different scattering geometries.

Through a well-known procedure of the first-order elasticity theory (see for instance Ref. 31), the unstrained lattice parameter of a layer (a_f) in heteroepitaxial structures can be expressed in terms of the misfit (m) and the Poisson ratio (ν). For a cubic crystal [001] oriented $\nu_{[001]}=c_{12}/(c_{11}+c_{12})$, with $c_{11,12}$ being elastic constants. In the case of a pseudomorphic growth the parallel mismatch component $(\Delta a/a_s)^{\parallel}=0$ and the relation becomes

$$m=\frac{a_f-a_s}{a_s}=\frac{1-\nu}{1+\nu}\frac{a_f^{\perp}-a_s}{a_s}=\frac{1-\nu}{1+\nu}(\Delta a/a_s)^{\perp},$$

where the subscript s is referred to the substrate parameter. Perpendicular mismatch components $(\Delta a/a_s)^{\perp}$ have been obtained both by the fitting of the 004 diffraction profiles and, through a well-known expression,[32] from the angular separation ($\Delta\theta$) between the GaAs substrate and MgS layer diffraction peaks, measured on the −224 RSM. For sample 1, the mismatch profile obtained by the fitting of the 004 reflection is not definitely convincing because the calculation works in a reliable way when the crystal is nearly perfect, and although the ZB bulk of the sample is pseudomorphic, the 004 diffraction profile shows a large broadening of the peaks due to the lattice disorder induced by the presence of RS cores and stacking faults. Then, the perpendicular mismatch component for this sample has been determined from the angular separation of both 004 and 224 Bragg reflections. The values $a_S=0.565\,35$ nm (see for instance Ref. 33), $\nu_{\text{ZnS}}=0.334$, and $\nu_{\text{MgS}}=0.433$ as obtained in this work from *ab initio* calculations (see next section) have been used for the GaAs substrate lattice parameter, ZnS and ZB-MgS Poisson ratio, respectively. From the analysis of all diffraction data the average value $(\Delta a/a)^{\perp}=-9.485\times10^{-3}$ has been found and the related lattice parameters are shown in Table I. The mismatch component was evaluated with an accuracy of $\pm5\times10^{-5}$ corresponding to an error of $\pm0.000\,015$ nm on the lattice parameter. The uncertainty on the Zn fraction $(0.005<x<0.02)$ incorporated in the MgS layer during the growth leads to the values $a_f(x)=0.563\,22$ nm for $x=0.005$ and $a_f(x)=0.563\,217$ nm for $x=0.02$, respectively, where f stands for ZB-$Zn_XMg_{1-X}S$ layer. The error associated with $(\Delta a/a)^{\perp}$ contains both the $a_f(x)$ values obtained for the two different compositions. The parameter (a_{MgS}) of the pure ZB MgS has been extrapolated by using the simple relation $a_f(x)=(1-x)\Delta a+a_{\text{ZnS}}$, with $\Delta a=a_{\text{MgS}}-a_{\text{ZnS}}$, under the hypothesis of a linear behavior $a_f(x)$ vs x (Vegard's law) and the assumption of $a_{\text{ZnS}}=0.5410$ nm for the ZB-ZnS lattice parameter.[34] Due to the variation in Zn fraction, the ZB-MgS lattice parameter is in the range $0.563\,33<a_{\text{MgS}}<0.563\,67$ nm. A comparison with some other experimental values will be given in Table III.

D. *Ab initio* calculations

The possibility of coexisting structural phases evidenced above is also in agreement with the theoretical predictions. From our calculations, for MgS, the perfect ZB and RS lattices are relatively close in energy, although evidently the RS structure is much more favorable than the ZB at equilibrium. The energy difference between the two structures is ~0.17 eV/f.u. [see Fig. 6(a)], which is entirely assigned to elastic energy. Indeed, we predict a reversed stability order for the corresponding pseudomorphic phases (*ps*), obtained by straining the lattice structure at equilibrium volume to the in-plane GaAs lattice parameter, adopted in the *ps* phase; the *ps*-RS structure is unfavorable by 0.8 eV/f.u. with respect to the *ps*-ZB, which is instead almost degenerate to the unstrained perfect ZB.

Beyond total energies and lattice parameters of the different structures, and alloys, it is possible to extract the bulk modulus and elastic constants from the *ab initio* results, as obtained from the shear/stress relation for small distortions around equilibrium, applying Hooke's law [see Fig. 6(b)].

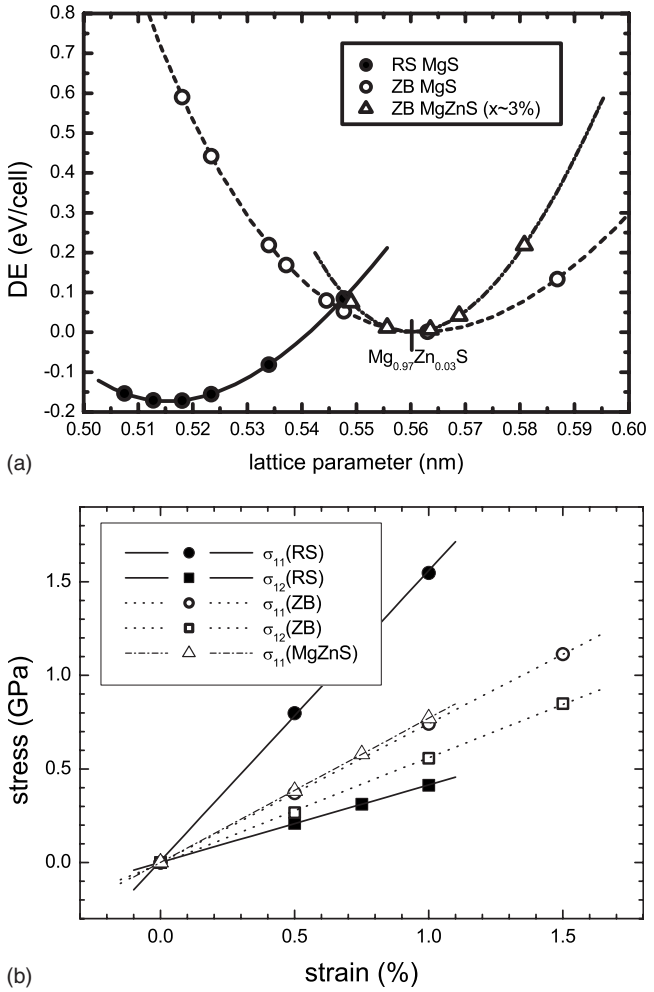

FIG. 6. Comparison of structural properties from *ab initio* calculations: (a) relative total-energy curve of the different crystal structures for MgS [closed (open) circle for rocksalt (zinc blende)] and predicted equilibrium lattice parameter for a 3% virtual-crystal $Zn_XMg_{1-X}S$ alloy; (b) stress as a function of strain for the rocksalt (closed symbols) and zinc-blende (open symbols) metastable phases and predicted σ_{11} for the 3% virtual-crystal $Zn_XMg_{1-X}S$ alloy; here $\sigma_{11}=\delta E/u_{xx}$ and $\sigma_{12}=\delta E/u_{xy}$ are obtained from *ab initio* total-energy (e) calculations, varying the lattice parameter in the corresponding directions.

This provides a predictive tool to obtain information for metastable phases not found in nature at equilibrium, free from assumptions on the underlying substrate lattices, or presence of dopants. The computed elastic constants are shown in Table II for the stable RS and the metastable ZB structures, and for template low Zn concentration virtual alloys in the ZB structure, at the respective equilibrium lattice parameter. Interestingly the alloy appears to be more rigid to shear deformations and much more compressive under hydrostatic pressures (smaller B_0) than the pure ZB phase, which is a hint for stabilizing Zn alloys in thin ZB films.[35] These constants, and in particular the Poisson ratio ν, have been used in the previous section to predict the lattice parameter of the ZnMgS alloy. The good consistency with the present experimental data validates the theoretical prediction and the methodology; it thus provides a good estimate for the elastic constants of ZB MgS, confirmed both by the experimental results and by comparison with similar calculations previously published (see Table III).

IV. SUMMARY AND CONCLUSIONS

A series of samples containing MgS layers with a small residual zinc mole fraction were grown by MBE at a temperature (300 °C) that was slightly above the known optimum temperature range (240–270 °C) in order to determine the effect on the structural properties of the material. This temperature is close to the maximum temperature at which this material can be successfully deposited. By comparison with previous samples grown at lower temperature (see for instance Ref. 6), it is possible to conclude that even if MgS could be grown also at 300 °C, as has been experimentally demonstrated in the present work, this temperature does not promote an improvement of the crystal quality of the whole structure. In this contest, the effect of the different buffer layers on the structure quality could not be emphasized. Despite a certain worsening of the structure, it was still possible to extract the lattice parameter of the ZB-MgS phase, which is one of the most important aims of this work. Using XRD and TEM methods we have fully characterized these MgS films, which were found to be ZB phase with RS inclusions, as induced by stress relief at phase boundaries. The coexistence of both RS and ZB-MgS structural phases was experimentally detected, and a partial nucleation of RS MgS was evidenced by both x-ray diffraction measurements and TEM investigations. The phase change was correlated with the presence of a high density of stacking faults and to their interaction. By collecting the x-ray coherent intensity distribution in the RSM it was possible to establish that the strain

TABLE II. Calculated elastic constants for the two different MgS lattices. c_{11} and Bulk parameter (B_0) from different *ab initio* calculations and Hooke's law, varying lattice parameters.

Lattice	c_{11} (GPa)	c_{12} (GPa)	B_0 (GPa)	Poisson	Young (GPa)	Shear (GPa)
RS	1.5511	0.4135	0.793	0.2105	1.377	0.569
ZB	0.742	0.5674	0.626	0.433	0.2508	0.0875
(Zn)MgS (3.1%)	0.759	0.55	0.6206	0.420	0.297	0.1045
(Zn)MgS (6.2%)	0.771	0.54	0.6166	0.411	0.316	0.116
ZnS	1.155	0.578	0.7703	0.3335	0.769	0.288

TABLE III. Comparison between our lattice ZB-MgS parameters and some previously published data.

			Calculated			Experimental	
c_{11} (GPa)	c_{12} (GPa)	ν	Ref.	a (nm)	Ref.	a (nm)	Ref.
7.237	5.57	0.435	36	0.5612	36	0.5590	3
8.84	4.80	0.352	37	0.5620	40	0.5660	4
7.40	5.47	0.425	38	0.5615	38	0.5622	6
5.68	5.79	0.505	39	0.5584	41	0.5619	42
7.42	5.67	0.433	Present work	0.5620 (LDA), 0.5670 (GGA)	Present work	0.56333, 0.56367	Present work

status of MgS ZB phase was pseudomorphic. This result allowed us to determine the ZB-MgS lattice parameter $0.563\,67 < a_{\mathrm{MgS}} < 0.563\,89$ nm, where the range is due to the uncertainty on the Zn fraction $(0.005 < x < 0.02)$ incorporated in the MgS layer during the growth, as determined by SIMS and Auger techniques. Our theoretical predictions allow us to provide a set of elastic constants for the otherwise unknown alloy, free from assumptions on the underlying substrate lattices. The theoretical and experimental sets of data for the lattice parameter in the allowed range of the alloy provide a consistent picture for the analysis of this artificial compound.

ACKNOWLEDGMENT

This work has been supported by the "SANDiE" Network of Excellence of EU under Contract No. NMP4-CT-2004-500101.

*bocchi@imem.cnr.it
†Present address: Physical Sciences, University of Cambridge, 25 Trumpington Road CB2 1QA, UK.

[1] N. Teraguchi, H. Mouri, Y. Tomomura, A. Suzuki, H. Taniguchi, J. Rorison, and G. Duggan, Appl. Phys. Lett. **67**, 2945 (1995).
[2] C. Bradford, C. B. O'Donnell, B. Urbaszek, A. Balocchi, C. Morhain, K. A. Prior, and B. C. Cavenett, Appl. Phys. Lett. **76**, 3929 (2000).
[3] K. Uesugi, T. Obinata, H. Kumano, J. Nakahara, and I. Suemune, Appl. Phys. Lett. **68**, 844 (1996).
[4] L. Konczewicz, P. Bigenwald, T. Cloitre, M. Chibane, R. Ricou, P. Testud, O. Briot, and R. L. Aulombard, J. Cryst. Growth **159**, 117 (1996).
[5] C. Bradford, C. B. O'Donnell, B. Urbaszek, A. Balocchi, C. Morhain, K. A. Prior, and B. C. Cavenett, Appl. Phys. Lett. **76**, 3929 (2000).
[6] C. Bradford, C. B. O'Donnell, B. Urbaszek, C. Morhain, A. Balocchi, K. A. Prior, and B. C. Cavenett, Phys. Rev. B **64**, 195309 (2001).
[7] M. Funato, A. Balocchi, C. Bradford, K. A. Prior, and B. C. Cavenett, Appl. Phys. Lett. **80**, 443 (2002).
[8] C. Bradford, B. Urbaszek, M. Funato, A. Balocchi, T. C. M. Graham, E. J. McGhee, R. J. Warburton, K. A. Prior, and B. C. Cavenett, J. Cryst. Growth **251**, 581 (2003).
[9] L. H. Kuo, L. Salamanca-Riba, B. J. Wu, G. E. H. Ofler, J. M. DePuydt, and H. Cheng, Appl. Phys. Lett. **67**, 3298 (1995).
[10] L. H. Kuo, K. Kimura, T. Yasuda, S. Miwa, C. G. Jin, K. Tanaka, and T. Yao, Appl. Phys. Lett. **68**, 2413 (1996).
[11] K. A. Prior, C. Bradford, L. David, X. Tang, and B. C. Cavenett, Phys. Status Solidi B **241**, 463 (2004).
[12] S. Takagi, Acta Crystallogr. **15**, 1311 (1962).
[13] D. Taupin, Bull. Soc. Fr. Mineral. Cristallogr. **87**, 69 (1964).
[14] A. Authier, *Ewald Waves in Theory and Experiment. Advances in Structure Research by Diffraction Methods*, edited by R. Brill and R. Mason (Vieweg und Sohn, Braunschweig, (1970).
[15] P. Giannozzi *et al.*, 2008, www.pwscf.org and www.quantum-espresso.org
[16] D. Vanderbilt, Phys. Rev. B **41**, 7892 (1990).
[17] J. P. Perdew and Y. Wang, Phys. Rev. B **45**, 13244 (1992).
[18] H. J. Monkhorst and J. D. Pack, Phys. Rev. B **13**, 5188 (1976).
[19] R. T. Moug, C. Bradford, and K. A. Prior, J. Korean Phys. Soc. **53**, 2996 (2008).
[20] D.-J. Kim, Y.-M. Yu, S.-H. Eom, T. H. Kim, C.-S. Go, and Y. D. Choi, Mater. Chem. Phys. **92**, 274 (2005).
[21] K. A. Prior, C. Bradford, L. David, X. Tang, and B. C. Cavenett, J. Cryst. Growth **275**, 141 (2005).
[22] L. Nasi, C. Bocchi, A. Catellani, F. Germini, J. K. Morrod, K. A. Prior, and G. Calestani, Appl. Phys. Lett. **91**, 111908 (2007).
[23] B. E. Warren, *X-Ray Diffraction*, Addison-Wesley Series in Metallurgy and Materials (Addison-Wesley, Reading, MA, 1969).
[24] P. F. Fewster, J. Appl. Crystallogr. **22**, 64 (1989).
[25] A. Navrotsky and J. C. Phillips, Phys. Rev. B **11**, 1583 (1975).
[26] P. F. Fewster, Appl. Surf. Sci. **50**, 9 (1991).
[27] H. Heinke, M. O. Moller, D. Hommel, and G. Landwehr, J. Cryst. Growth **135**, 41 (1994).
[28] N. Wang, K. K. Fung, and I. K. Sou, Appl. Phys. Lett. **77**, 2846 (2000).
[29] J. Tanimura, O. Wada, T. Ogama, Y. Endoh, and M. Imaizumi, J. Appl. Phys. **77**, 6223 (1995).
[30] K. A. Prior, S. A. Telfer, X. Tang, C. Morhain, B. Urbaszek, C. O'Donnell, P. Tomasini, A. Balocchi, and B. C. Cavenett, J. Cryst. Growth **227-228**, 655 (2001).
[31] C. Kittel, *Introduction to Solid State Physics* (Wiley, New York, 1966), Chap. 4.
[32] C. Bocchi and C. Ferrari, J. Phys. D **28**, A164 (1995).
[33] A. Navarro-Quezada, A. G. Rodriguez, M. A. Vidal, and H.

Navarro-Quezada, J. Cryst. Growth **291**, 340 (2006).
[34] J. C. Jamieson and H. H. Demarest, J. Phys. Chem. Solids **41**, 963 (1980).
[35] C. Bradford, R. T. Moug, A. Curran, D. Thuau, R. J. Warburton, and K. A. Prior, J. Korean Phys. Soc. **53**, 3000 (2008).
[36] F. Drief, A. Tadjer, D. Mesri, and H. Aourag, Catal. Today **89**, 343 (2004).
[37] P. K. Jha and M. Talati, Phys. Status Solidi B **239**, 291 (2003).
[38] D. Wolverson, D. M. Bird, C. Bradford, K. A. Prior, and B. C. Cavenett, Phys. Rev. B **64**, 113203 (2001).
[39] Tae-Young Chung, J. H. Oh, Sun-Ghil Lee, Ji-Wook Jeong, and K. J. Chang, Semicond. Sci. Technol. **12**, 701 (1997).
[40] Y. Morinaga, H. Okuyama, and K. Akimoto, Jpn. J. Appl. Phys., Part 1 **32**, 678 (1993).
[41] S. G. Lee and K. J. Chang, Phys. Rev. B **52**, 1918 (1995).
[42] R. W. G. Wyckoff, *Crystal Structures* (Wiley, New York, 1963).